• Original Paper •

Application of a Three-dimensional Variational Method for Radar Reflectivity Data Correction in a Mudslide-inducing Rainstorm Simulation

Hongli LI[*1,2,3] and Xiangde XU[1]

[1]*State Key Laboratory of Severe Weather, Chinese Academy of Meteorological Sciences, Beijing* 100081, *China*
[2]*Nanjing University of Information Science and Technology, Nanjing* 210044, *China*
[3]*Hubei Key Laboratory for Heavy Rain Monitoring and Warning Research, Institute of Heavy Rain,*
China Meteorological Administration, Wuhan 430205, *China*

ABSTRACT

Various types of radars with different horizontal and vertical detection ranges are deployed in China, particularly over complex terrain where radar blind zones are common. In this study, a new variational method is developed to correct three-dimensional radar reflectivity data based on hourly ground precipitation observations. The aim of this method is to improve the quality of observations of various types of radar and effectively assimilate operational Doppler radar observations. A mudslide-inducing local rainstorm is simulated by the WRF model with assimilation of radar reflectivity and radial velocity data using LAPS (Local Analysis and Prediction System). Experiments with different radar data assimilated by LAPS are performed. It is found that when radar reflectivity data are corrected using this variational method and assimilated by LAPS, the atmospheric conditions and cloud physics processes are reasonably described. The temporal evolution of radar reflectivity corrected by the variational method corresponds well to observed rainfall. It can better describe the cloud water distribution over the rainfall area and improve the cloud water analysis results over the central rainfall region. The LAPS cloud analysis system can update cloud microphysical variables and represent the hydrometeors associated with strong convective activities over the rainfall area well. Model performance is improved and the simulation of the dynamical processes and moisture transport is more consistent with observation.

1. Introduction

Mesoscale convective clouds often develop rapidly and with complex structure. They interact in multiple ways with the environmental background as well as cloud microphysical processes. Highly unstable atmospheric conditions and triggering mechanisms that lead to ascending motion are prerequisites for the development of convective clouds. Clouds and precipitation are primarily composed of discrete liquid or solid particles, including cloud and rain droplets, snow crystals, snowflakes, sleet and hails. The formation and growth of these particles is actually the result of interactions between thermodynamic processes and microphysical processes in the atmosphere (Reisner et al., 1998; Zhang et al., 2009; Zheng et al., 2013). The development of strong convective cloud is often accompanied by heavy rain, hail and other mesoscale disastrous weather. Our understanding of cloud physics and precipitation processes is insufficient due to their complexity and diversity, which leads to inappropriate descriptions of the physical processes involved in clouds and precipitation in numerical models. This is one of the major reasons for the uncertainty in numerical modeling studies (IPCC, 2001).

In order to reduce the spin-up problem in numerical models, it is necessary to introduce atmospheric water vapor content and other hydrometeors into the initial conditions of numerical models (Xue et al., 2003; Barker et al., 2004; Liu et al., 2008). However, regular atmospheric observations cannot provide the hydrometeor fields required as the input for data assimilation systems. For this reason, a cloud analysis system is often applied to produce the hydrometeor fields involved in cloud physics and rainstorms. Currently, several widely used cloud analysis systems include LAPS (Local Analysis and Prediction System), ADAS (ARPS Data Analysis System; ARPS refers to Advanced Regional Prediction System) and GRAPES-MESO (Global/Regional Assimilation and Prediction System mesoscale numerical forecast system). Hu et al. (2006a, b) implemented the ADAS cloud analysis system to

---

* Corresponding author: Hongli LI
  Email: lihongli@whihr.com.cn

assimilate observations from operational WRS-88D Doppler radars in their simulation of clusters of tornadic thunderstorms using the mesoscale modeling system ARPS. It was found that the experiment using the improved ADAS cloud analysis procedure with reflectivity could capture important characteristics of the main tornadic thunderstorms more accurately. With assimilation of radar observations, the spin-up problem in storm prediction can be significantly reduced and the storm cluster can be forecasted two hours earlier than without assimilation. Qu et al. (2012) designed the GRAPES-MESO cloud analysis system and applied it to the assimilation of the blackbody temperature and total cloud amount derived from satellite images provided by the Feng-Yun II geostationary satellite. The results of typhoon simulations indicated that the GRAPES-MESO cloud analysis system can retrieve three-dimensional cloud cover information reasonably well. LAPS, developed by NOAA since the 1990s, was the first cloud analysis system to implement a multiple iteration successive corrections method. LAPS can assimilate regular soundings, surface observations, radar reflectivity analysis, satellite image products of all channels, standard aviation routine weather reports, multi-layered CO_2 products etc., to produce high spatiotemporal resolution cloud fields, including three-dimensional cloud views, two-dimensional cloud coverage, cloud base and cloud top heights, and cloud water/ice mixing ratios (Albers et al., 1996). Shaw et al. (2001) conducted hot-start numerical studies using the LAPS cloud analysis products in their initialization, and improved the first three hours' forecast skill scores.

The implementation of a cloud analysis system can provide cloud parameters such as cloud water content and cloud ice content for the initial conditions of numerical models. However, the accuracy of cloud analysis systems depends on multisource and high spatiotemporal resolution observations, such as satellite remote sensing data and radar observations. With the development of the weather observation network in China, an increasing number of new detection instruments, mainly composed of operational weather Doppler radar, have been deployed to obtain real-time and high spatiotemporal resolution observations. The unique advantages of Doppler radar in high-resolution mesoscale detection, which includes the detection of three-dimensional clouds, precipitation and wind, provide the possibility for successful cloud analysis. LAPS combines data from different sources to analyze clouds and hydrometeors to produce thermodynamically balanced initial conditions for numerical models, and thereby improves short-range precipitation forecasts (Albers et al., 1996; Xie et al., 2013). Researchers in China have implemented LAPS to integrate multiple sources of observations and found that the accuracy of the cloud analysis depends on the accuracy of the high-resolution radar reflectivity and the reliability of the satellite remote sensing data (Li et al., 2009; Liu et al., 2014).

Various types of Doppler radars with different horizontal and vertical detection ranges are deployed. How to improve the quality of data from different types of radars and effectively assimilate these data in the LAPS cloud analysis system to provide reasonable initial conditions of cloud

fields is critical for the improvement of mesoscale model forecasts of local rainstorms. Southwest China is characterized by complex terrain with mountains and rolling hills. Heavy precipitation is frequent in Southwest China, which often leads to mudslides, landslides and other secondary geological disasters, and subsequent serious losses to human life and the economy. For example, Wangmo County in Guizhou Province has experienced mountain torrents and mudslides many times in the past, and short-term intense rains are the main trigger of the mudslides. Previous studies have indicated that heavy rainstorms able to induce secondary geological disasters (e.g., mudslides) share common features; for instance, they all last for a short time, their rainfall intensity is high, and their heavy rainfall is highly localized. These heavy rainstorms often appear as local abnormal precipitation on small scales (Xu et al., 2005; Zhao and Cui, 2010; Li et al., 2014). So far, studies on data quality control, especially for radar observations in Southwest China, have been conducted. However, the unique landscape in Southwest China imposes limitations on the effective radar detection range in both the horizontal and vertical direction. The uncertainties of the strong three-dimensional radar signals in the radar mosaic add difficulty to the application of LAPS in the reanalysis of the cloud physical processes involved in micro- and mesoscale rainstorms and mudslides.

The regional ground rain gauge stations of the China Mesoscale Observation Network can compensate well for the missing information in radar blind zones. Continuous hourly precipitation can be directly measured by ground rain gauges with high accuracy at each individual station. However, ground rain gauge measurements often miss the heavy precipitation center due to the inhomogeneous distribution of weather stations and precipitation. Radar can detect real-time clouds and precipitation structure and the evolution of the precipitation system, and quickly provide the real-time spatial distribution of the precipitation within a certain area (Zhang et al., 2007). The relationship between rain rate and radar reflectivity is the basis for the quantitative radar measurement of precipitation. Using the variational method, the three-dimensional radar mosaic can be corrected based on real-time precipitation observations. This method is effective for solving the problems caused by blind zones of various types of radar, and problems related to the quality of the radar mosaic. As a result, the fusion effects of radar reflectivity in the LAPS cloud analysis can be improved, leading to a more realistic description of cloud microphysical parameters in the initial conditions of numerical models, and improvement in the simulation of local heavy precipitation on the micro- and mesoscale.

In the present study, the LAPS cloud analysis system and the Weather Research Forecast (WRF) model are applied to simulate local heavy precipitation events that occurred in Wangmo County, Guizhou Province. A variational method is implemented to correct the three-dimensional radar reflectivity based on ground rain gauge observations. The improvement in the simulation of local heavy precipitation events of this type through application of radar radial velocity and re-

flectivity data and the variational method is investigated. The purpose of the study is to more effectively assimilate radar reflectivity information into the initial conditions of models, besides radial velocity, and improve the performance of the numerical simulation of mesoscale rainstorms.

2. Principles of the variational method for radar reflectivity correction

According to the variational principle, the functional J of several independent variables (x,y) can be written as

$$J[U(x,y)] = \iint F\left(x,y,U,\frac{\partial U}{\partial x},\frac{\partial U}{\partial y}\right)\mathrm{d}x\mathrm{d}y , \qquad (1)$$

in which F is the function, and $U(x,y)$ is the dependent variable of x and y. $U(x,y)$ must satisfy the Eulerian equation

$$FU - \left(\frac{\partial}{\partial x}FU_x + \frac{\partial}{\partial y}FU_y\right) = 0 . \qquad (2)$$

Assume that the gridded three-dimensional radar reflectivity at each grid (x,y) in the study area is $Z_{A_k}(x,y)$, where k is the vertical level and A_k is the gridded analysis value at k level. If $Z_{G_k}(i,j)$ is the corresponding reflectivity retrieved from hourly ground rain gauge observations at the location (i,j) at k level, then the difference between $Z_{G_k}(i,j)$ and $Z_{A_k}(x,y)$ is the error field $\widetilde{C_k}(i,j)$ at k level at (i,j), which can be expressed as

$$\widetilde{C_k}(i,j) = Z_{G_k}(i,j) - Z_{A_k}(i,j) . \qquad (3)$$

It is necessary to construct a broad bias correction function due to the limited number of ground stations. When using the variational method to obtain $C_k(x,y)$ at k level at (x,y), the following functional J must reach its minimum value.

$$J = \iint (C_k - \widetilde{C_k})^2 \mathrm{d}x\mathrm{d}y . \qquad (4)$$

That is, $\sum_i \sum_j (C_k - \widetilde{C_k})^2$ must reach its minimum value.

For the above variational problem, the following functional J is constructed:

$$J = \iint \left\{(C_k - \widetilde{C_k})^2 + \lambda \left[\left(\frac{\partial C_k}{\partial x}\right)^2 + \left(\frac{\partial C_k}{\partial y}\right)^2\right]\right\}\mathrm{d}x\mathrm{d}y , \qquad (5)$$

where λ is the constraint factor. The first-order partial derivative of Eq. (5) can be written as

$$\delta J = \delta \sum_x \sum_y \left\{(C_k - \widetilde{C_k})^2 + \lambda \left[\left(\frac{\partial C_k}{\partial x}\right)^2 + \left(\frac{\partial C_k}{\partial y}\right)^2\right]\right\} . \qquad (6)$$

The necessary condition for J to reach its extreme values, Eq. (5), is $\delta J = 0$, and the corresponding Eulerian equation is

$$(C_k - \widetilde{C_k}) - \widetilde{\lambda}\left[\frac{\partial^2 C_k}{\partial x^2} + \frac{\partial^2 C_k}{\partial y^2}\right] = 0 , \qquad (7)$$

where $\widetilde{\lambda}$ is strain constraint factor, or Lagrangian multipliers, which is introduced into Eq. (7) to obtain the extrema of function J. For each vertical level k, the numerical solution to the above equations can be obtained iteratively. After the correction based on the variational method is complete, we obtain the new three-dimensional bias correction function $C_k(x,y)$. The corrected three-dimensional radar reflectivity factors are expressed as

$$\begin{pmatrix} Z_1(x,y) \\ Z_2(x,y) \\ \cdots \\ Z_k(x,y) \end{pmatrix} = \begin{pmatrix} Z_{A_1}(x,y) + C_1(x,y) \\ Z_{A_2}(x,y) + C_2(x,y) \\ \cdots \\ Z_{A_k}(x,y) + C_k(x,y) \end{pmatrix} . \qquad (8)$$

Observations of multiple radars are interpolated into the LAPS three-dimensional grids to obtain the gridded radar reflectivity $Z_{A_k}(x,y)$ within our study domain. The reflectivity factor $Z_G(i,j)$, retrieved from hourly ground rain gauge observations, is obtained by finding the optimum coefficient in the dynamic relationship of the rain rate I and the radar reflectivity factor Z. In previous studies, an exponential relationship between the rain rate and radar reflectivity factor was identified. Various calibration methods, e.g. the average calibration method, the Kalman filter calibration method, the optimal interpolation method, the variational method, and the statistical weight calibration method, have been applied to estimate grouped Z–I relations. Results indicate that compared with other Z–I relations, the dynamic Z–I relation can better fit rainfall estimated from radar observations with ground observations (Chiang et al., 2007). Suppose that the rain rate $I_G(i,j)$ at each rain gauge station (i,j) corresponds to a radar reflectivity factor dBZ, then dBZ can be used to derive the rain rate based on the relationship between the radar reflectivity factor and rainfall intensity, i.e. $Z = aI^b$. Through time integration of this rain rate, the hourly precipitation $I_R(i,j)$ estimated from radar observations can be determined. To obtain the optimal values of coefficients a and b in the dynamical relationship Z–I, the discriminant function $\mathrm{CTF} = \sum_i \sum_j |I_G(i,j) - I_R(i,j)|$ is established. First, assign initial values to a and b; then, change a and b within a certain range until CTF reaches its minimum value, meanwhile achieving the optimum values of a and b at each vertical level. Based on the Z–I relationship (a and b set at optimal values at each vertical level), and the hourly rain gauge observations $I_G(i,j)$, the radar reflectivity factor $Z_{G_k}(i,j)$ at each level over the corresponding weather station can be retrieved.

3. Radar data and numerical experiment design

During the period 5–6 June 2011, significant precipitation occurred over Guizhou Province under the combined effects of an upper-level trough and a lower-level shear line. Figure 1a shows the 24-h accumulated rainfall observed from 0000 UTC 5 June to 0000 UTC 6 June 2011 (the same hereafter). Specifically, on the early morning of 6 June, short-term intense precipitation occurred over Wangmo County in

southern Guizhou Province, with heavy and extremely heavy precipitation over several towns. Twelve-hour (1200 UTC 5 June to 0000 UTC 6 June) accumulated precipitation larger than 80 mm was observed at Dayi (315 mm), Xintun (127.6 mm), Barao (113.2 mm), Kanbian (87.4 mm) and Jiaona (80.9 mm). The largest 1-h rainfall occurred at 1500 UTC in Wangmo County (Fig. 1b). Such heavy precipitation led to clustered large-scale mudslides, mainly over the northern mountainous region of Wangmo County, including the upstream areas of Dajian River, Dayi River, and Lewang River, where heavy precipitation centers were located.

In this study, an integrated assimilation–forecast system, in which LAPS is used as the data assimilation system and WRF as the weather forecast model, is implemented for numerical experiments. With a horizontal resolution of 3 km × 3 km, the domain covers 501×401 grids in the east–west and north–south directions, with its center at (25.5°N, 105.5°E).
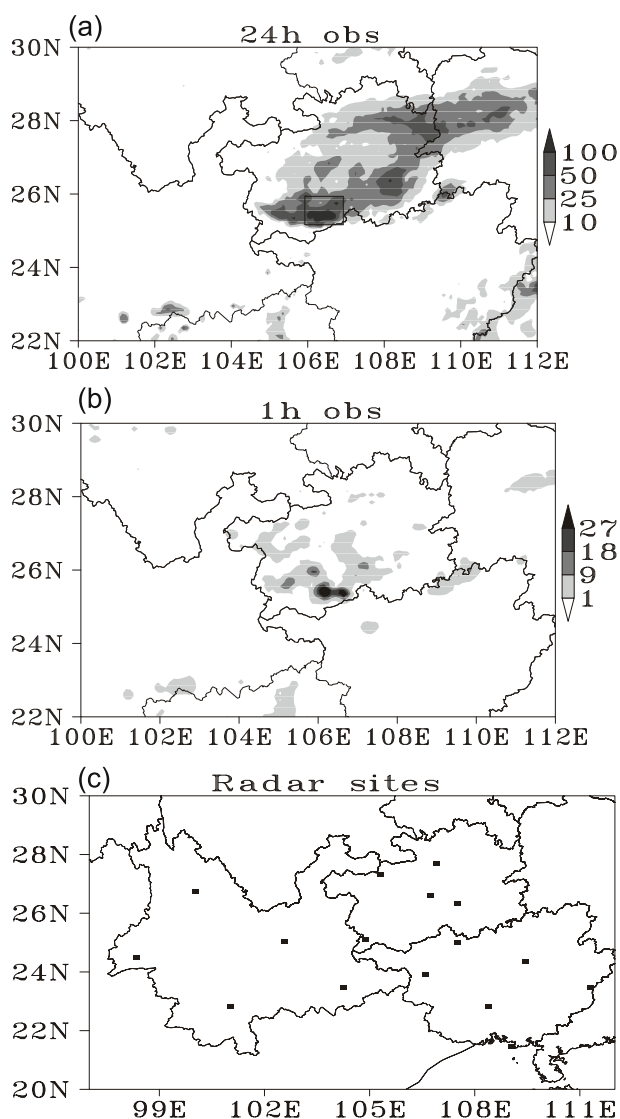

Fig. 1. The (a) 24-h observed rainfall from 0000 UTC 5 June 2011 to 0000 UTC 6 June 2011 (units: mm), (b) 1-h observed rainfall at 1500 UTC 6 June (units: mm), and (c) radar distribution in the study area.

In the vertical direction, the model's top is set at 50 hPa, with 42 layers. The main physics options include the RRTM longwave radiation scheme, the Goddard shortwave radiation scheme, the YSU (Yonsei University) boundary layer scheme, and the WSM6 microphysics scheme. Cumulus parameterization is turned off in this study due to the high resolution of 3 km. The assimilated radar data are extracted from 16 radar observations. These radars are of different types and deployed in Guizhou, Yunnan, and Guangxi provinces (Fig. 1c). Five C-band radars are located at Guiyang, Zunyi, Douyun, Bijie, and Xingyi; another five C-band radars are deployed at Kunming, Dehong, Wenshan, Simao, and Lijiang; and the remaining six S-band radars are deployed at Guilin, Nanning, Liuzhou, Beihai, Baise, and Hechi. The preprocessor of LAPS is utilized to preprocess the radar data, including threshold analysis, noise filtering, three-dimensional interpolation, smoothing, and missing data filling. After the quality control and spatial interpolation, the final radar reflectivity factor dataset is output in the format accepted by LAPS. The real-time hourly gridded precipitation observations provided by China Meteorological Information Center (Shen and Xiong, 2015) are used to verify the model results.

In order to investigate the effects of the variational method in improving the numerical simulation results, four experiments, referred to as NORA, RV, RA and RNRA, are carried out in this study. In the NORA experiment, data assimilation is not activated. The initial and boundary conditions are derived from the FNL analysis at 0000 UTC 5 June 2011, and WRF is integrated for 24 hours. In the other three assimilation experiments, the FNL analysis at 0000 UTC 5 June 2011 is taken as the background. In the RV experiment, radar radial velocity and zero reflectivity data are assimilated by LAPS, which is activated to generate the initial condition for a 24-h WRF integration. In the RA experiment, both radar radial velocity and reflectivity factor data are assimilated by LAPS. The RNRA experiment is the same as the RA experiment, except that the radar reflectivity factor data that have been corrected based on hourly rainfall observations at ground stations are assimilated by LAPS. Lateral boundary forcing for all three experiments is derived from the hourly FNL analysis on global 1° × 1° grids.

4. Results

4.1. *Response of three-dimensional radar reflectivity to rainfall*

Figure 2 shows scatter plots of hourly rainfall and radar reflectivity before and after variational correction at different levels. The distribution patterns are similar at each level. However, before the correction, radar echoes and hourly rainfall are highly disperse, with small correlation coefficients of 0.13, 0.16 and 0.18 at 925 hPa, 850 hPa and 700 hPa respectively; whereas after the correction, hourly ground rainfall and radar echoes demonstrate a distinct exponential relationship, with correlation coefficients of 0.54, 0.57 and 0.56 at 925 hPa, 850 hPa and 700 hPa, respectively. This result
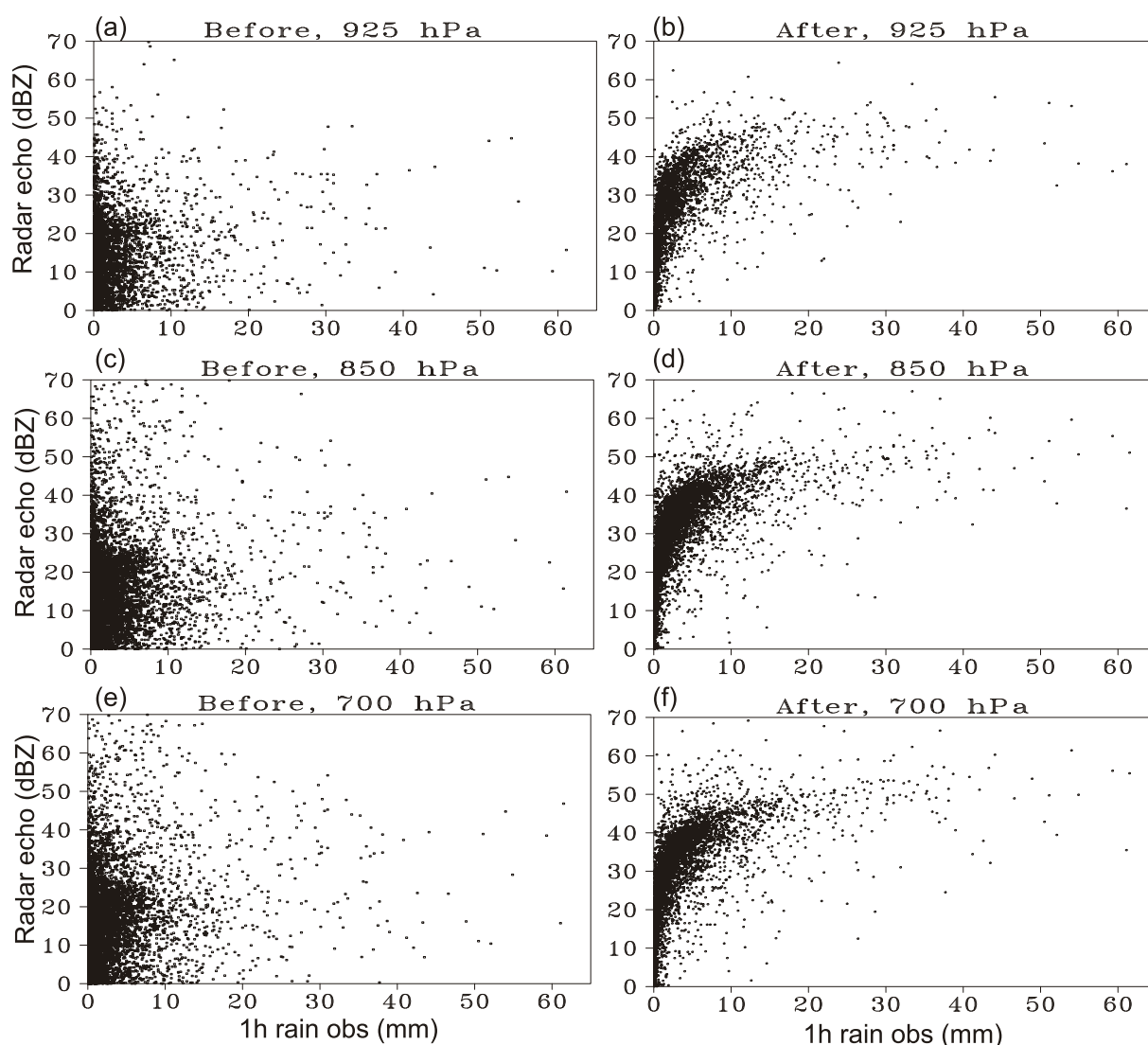
Fig. 2. Scatterplots of rainfall observations and radar echoes (a, c, e) before and (b, d, f) after the correction using the variational method, for the period 0000 UTC 5 June to 2300 UTC 5 June 2011: (a, b) 925 hPa; (c, d) 850 hPa; (e, f) 700 hPa.

clearly indicates that the variational method can efficiently incorporate rainfall information in the radar echoes.

Meanwhile, differences in radar reflectivity before and after the correction at different times indicate that the radar reflectivity field is corrected. From lower to upper levels, the range of correction is related to the rainfall amount and rainy area. Positive bias occurs in areas of large precipitation, and the variational correction is carried out at all levels. In the LAPS cloud analysis system, cloud coverage, cloud water content and cloud ice content etc. are corrected using radar reflectivity data. Thereby, it is important to investigate the effects of radar reflectivity correction based on hourly rainfall observations, which will significantly affect the evolution of cloud fields during the rainstorm processes. Figure 3 shows time–height cross sections of hourly rainfall at Wangmo, the center of the rainstorm, and LAPS radar echoes before and after the correction. The rainstorm started at 1200 UTC 5 June 2011 and continued until 2300 UTC. The largest rainfall intensity occurred at 1500 UTC, with hourly pre-

cipitation of 60 mm (Fig. 3a). The radar echoes before the bias correction corresponded to observed rainfall, and strong radar echoes located above the center of precipitation with maximum radar echo occurred at 1500 UTC (Fig. 3b). After the bias correction, the distribution of radar echoes was similar to that before the bias correction, but the echo intensity and vertical range were adjusted to be more consistent with the amount of rainfall. At 1100 UTC, precipitation was small and the radar echo was decreased. The largest precipitation occurred during 1500–1700 UTC, while the radar echo intensity and vertical range increased correspondingly. A similar situation can also be observed during 2000–2300 UTC, when the second largest precipitation occurred (Fig. 3c). The distribution of the differences in radar echoes before and after the bias correction is similar to that of rainfall. During the period of heavy precipitation, strong convection developed and the radar echo difference was positive above the center of precipitation. Apparently, the bias correction using the variational method increased the radar echo above
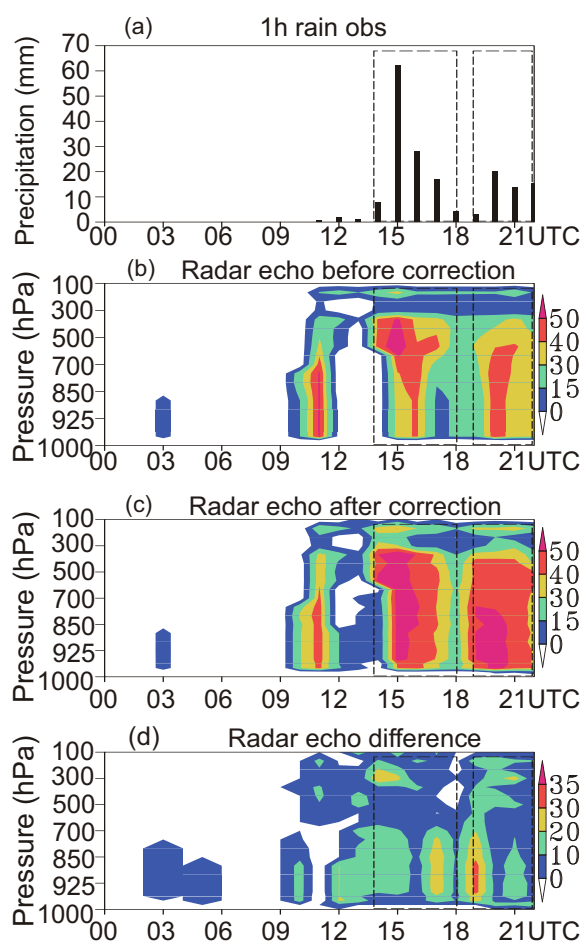
Fig. 3. Time–height cross sections of (a) rainfall at Wangmo Station, which is located at the center of the rainstorm (units: mm); (b) radar echoes (units: dBZ) before the variational correction; (c) radar echoes after the variational correction (units: dBZ); and (d) the difference between the radar echoes of before and after the correction (units: dBZ). The black dotted rectangle represents the time period of the strong precipitation.

the heavy rainfall area (Fig. 3d). The above analysis suggests that the temporal evolution of the corrected radar reflectivity is more consistent with the hourly rainfall than that of the original radar reflectivity. This is favorable for further studies of cloud physics based on the results of the LAPS cloud analysis system, which assimilates radar data.

4.2. *LAPS cloud microphysics analysis*

Cloud water content, cloud ice content and rainwater content etc. cannot be measured directly. However, changes in aqueous phases in the physical processes described in numerical models affect the model capability. Accurate moisture fields in the initial conditions are important for the "hot-start" and the improvement of model performance. The cloud mixing ratio is a key parameter in cloud physics and precipitation processes. Changes in atmospheric cloud water content actually reflect changes in cloud physics. The LAPS cloud analysis uses radar reflectivity to revise cloud hydrometeors.

Comparing hourly rainfall observations and cloud hydrometeors analyzed by LAPS in RA and RNRA, respectively, the LAPS output of the three-dimensional distribution of cloud water content before and after the variational correction is similar to that of the differences in radar echo. Application of the variational method can revise the structure of the cloud water distribution and improve the analysis of cloud water over the central precipitation region.

The temporal evolutions of cloud water content, cloud ice content and rainwater content (Fig. 4) analyzed by LAPS before and after the variational correction show that, at the time of heavy precipitation, the maximum value of the cloud water mixing ratio before the correction is 1.8 g kg^{-1}, whereas after the correction it is 2.4 g kg^{-1}. This is consistent with the fact that cloud water content is larger during the heavy rainfall period. Cloud ice and rainwater contents show features similar to cloud water content. The layer of large cloud ice mixing ratio is thicker after the correction than it is before the correction. The maximum rain water mixing ratio before the correction is 1.2 g kg^{-1} at the time of heavy precipitation, but the value becomes 2.1 g kg^{-1} after the correction. This result indicates that, after the variational correction, the LAPS cloud analysis output is capable of describing the more abundant cloud hydrometeors distributed over the rainfall area, therefore providing moisture contents that are more consistent with real-time precipitation processes for the model initial condition.

4.3. *WRF–LAPS initial conditions*

The LAPS wind analysis combines Doppler radar radial velocity and other wind observations into a three-dimensional gridded wind field (Albers, 1995). Radar reflectivity and other observations are assimilated in the LAPS cloud analysis to give the cloud fraction of each grid. Then, LAPS makes moisture analysis with the cloud fraction output (Birkenheuer, 1999). Finally, LAPS makes an adjustment to the basic model elements such as temperature, pressure, humidity and wind, based on certain constraints in the LAPS balance analysis (McGinley et al., 1991). In LAPS, various fields are first analyzed individually (univariately). The LAPS balance step uses the three-dimensional variational method to bring the mass field (geopotential height) and winds (u, v) into balance by minimizing the residual in the equations of motion. Depending on a scaling parameter, the balance may be quasi-geostrophic or fully nonlinear terms. As the scales of interest get smaller (mesoscale), one should include more impact of the nonlinear terms. The balance package also imposes mass continuity as a constraint. It ensures that the continuity is satisfied at all grid points. Good correspondence between the wind and heights is achieved after the balance. So, once one basic model element is adjusted after data assimilation in the initial fields of the model made by LAPS, the other model elements are adjusted according to the LAPS balance procedure analysis.

From the distribution of 1-h rainfall at the initial time (0000 UTC 5 June), the rainy areas lie in the east of Guizhou Province (Fig. 5a). In RA, with radar reflectivity assimilated
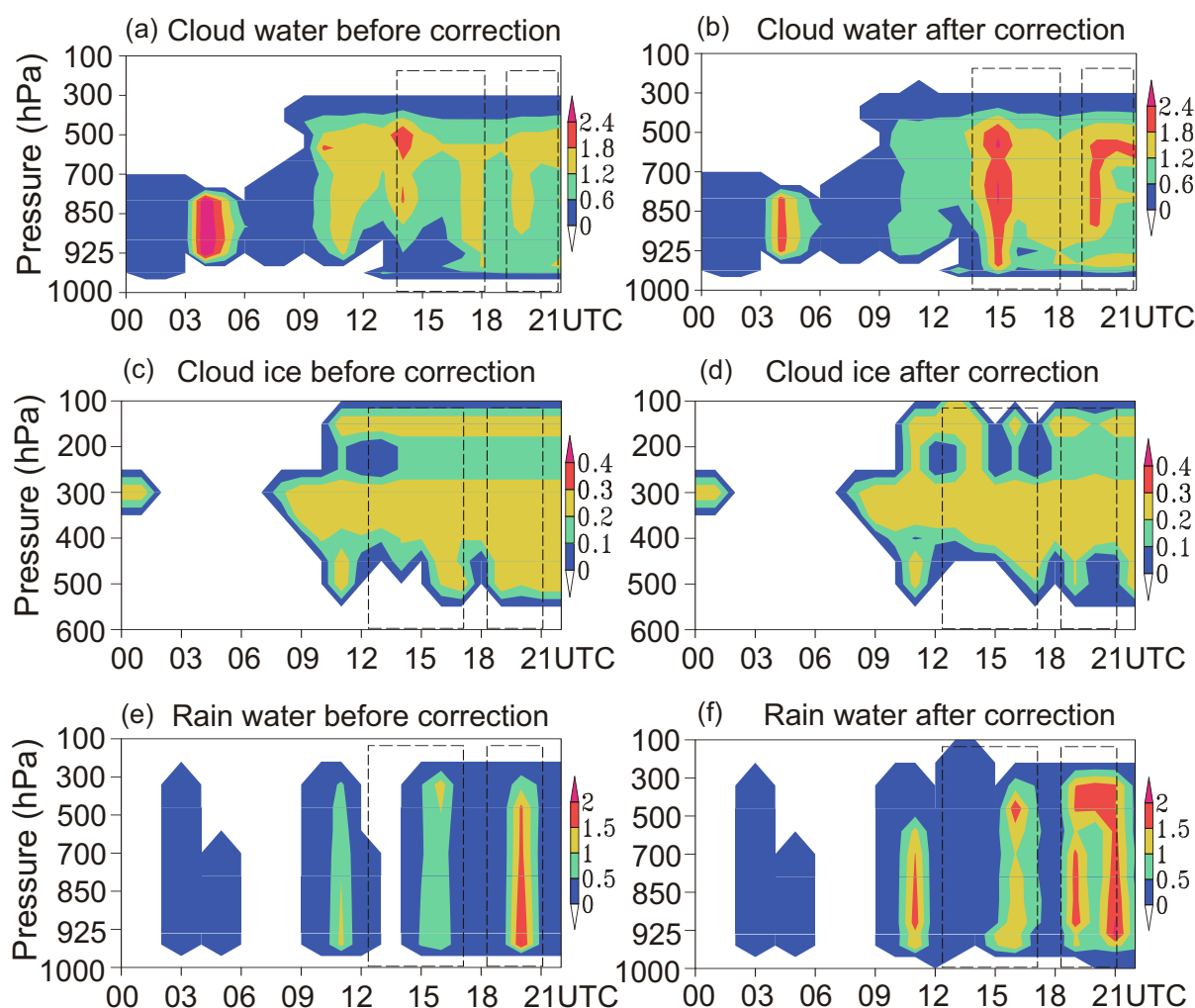
Fig. 4. Time–height cross sections of (a, b) cloud water, (c, d) cloud ice, and (e, f) rain water from the LAPS output (units: g kg^{-1}): (a, c, e) before correction; (b, d, f) after correction. The black dotted rectangle represents the time period of the strong precipitation.

in LAPS, the radar echoes still exist in the same areas (Fig. 5b). Comparing the LAPS analysis of radar echoes before and after the variational correction (Figs. 5b and c) at the initial time of this mudslide-inducing rainstorm experiment, it can be found that, before the variational correction, the maximum radar reflectivity distribution for the RA experiment shows that the areas of large radar reflectivity correspond to the areas of hourly precipitation in east Guizhou Province. After correction through the variational method, radar echoes are increased over rainy areas based on real-time observations of rainfall for the RNRA experiment. Meanwhile, with radar radial velocity assimilated by the LAPS wind analysis, and the wind fields adjusted by the LAPS balance analysis, the wind fields at the upper levels over the rainy areas are also corrected to a certain degree by assimilating radar reflectivity, regardless of whether or not this variational method is used (Figs. 5d and e). The difference in the RA and RV 850-hPa wind fields shows that the wind field is modified greatly in radar echo areas and less so in other areas when assimilating radar reflectivity by LAPS. The difference in the RNRA

and RA 850-hPa wind fields shows that the wind fields are mainly modified in the rainy area (Fig. 5e). Atmospheric humidity increases at the low level over the rainy area (Fig. 5f), indicating that the radar reflectivity assimilation by LAPS after variational correction can adjust the initial condition by adding to it hourly rainfall observations.

4.4. *Impact of the WRF–LAPS model simulation precipitation results*

The above analysis shows that the variational method can correct all the basic elements and cloud microphysical variables in the LAPS analysis. The question then arises as to whether the model performance can be improved if LAPS is implemented to provide the initial condition for the numerical model simulation. Comparison of the 24-h accumulated precipitation simulated by the four experiments (Fig. 6) with rainfall observation (Fig. 1a) shows that precipitation was mainly concentrated over Guizhou and western Hunan Province, and the two heavy precipitation centers in Guizhou Province were located at southeastern and south-
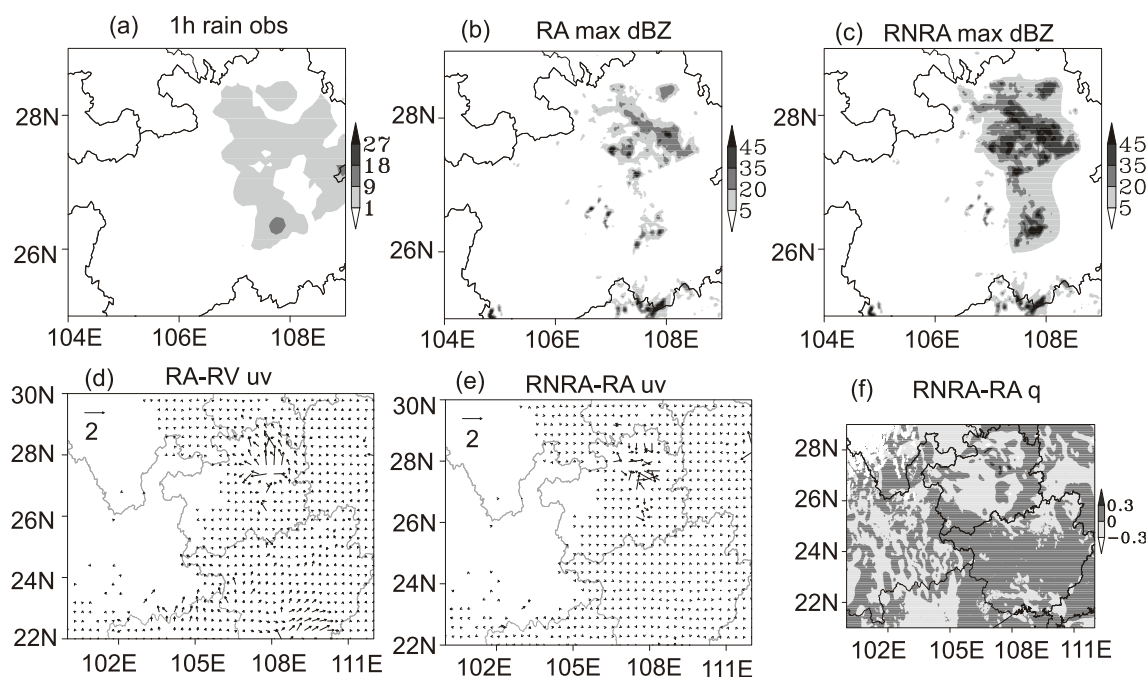
Fig. 5. The (a) 1-h rainfall distribution (units: mm) and the (b, c) maximum radar reflectivity in (b) RA and (c) RNRA at 0000 UTC 5 June 2011 (units: dBZ), the (d, e) difference in the 850 hPa wind fields between (d) RA and RV and (e) RNRA and RA (units: m s^{-1}), and the (f) difference in 700 hPa humidity between RNRA and RA (units: g kg^{-1}).

western (Wangmo) Guizhou, respectively. The four experiments can simulate the precipitation regions over Guizhou, but the NORA experiment, without assimilation of radar data, overestimates the rainfall over large areas of southern Guizhou and cannot reproduce precipitation over large areas of northeastern Guizhou, where the simulated precipitation is far more than the observed precipitation. In northern Guangxi Province, the NORA experiment overestimates the precipitation. The other three assimilation experiments, i.e. RV, RA and RNRA, can successfully correct the overestimated precipitation in southern Guizhou, and slightly improve the precipitation forecast in eastern Guizhou. However, they also overestimate the precipitation in the southern and eastern portions of the model domain (Guangxi Province), which is similar to the NORA experiment. In this rainstorm case, the radar data assimilation by LAPS is helpful for improving the precipitation simulation in the heavy rainfall area, but cannot remove the overestimated precipitation in some areas of the southeastern model domain. The initial wind fields of the experiments indicate that adjustment in the rainy area is large, while little is found in the southeastern portion of the model domain. This shows that assimilating radar data by LAPS cannot effectively adjust the background fields of this area. Thereby, sensitivity experiments with more rainstorm cases should be conducted to optimize LAPS for assimilating radar data.

Compared with the other experiments, RNRA can better simulate the extremely heavy precipitation (central precipitation amount above 100 mm) that occurred at Wangmo, which is our major concern in this study. The simulated rainfall in-

tensity and location are consistent with observations. In addition, the rainstorm center in southeastern Guizhou and the area of precipitation in northeastern Guizhou are also well simulated. The 24-h precipitation forecast threat score (TS) (Fig. 6e) results show that, except for light precipitation, the TS of the RNRA experiment remains higher than that of the other experiments. Specifically, the RNRA TS for the rainstorm simulation is the highest among all four experiments. Looking at the forecast errors (Fig. 6f), it can be seen that the largest error occurs in the simulation of NORA, mainly because it falsely simulates the observed precipitation over a large area. The forecast errors in the simulations of the other three assimilation experiments are similar for heavy and extremely heavy rain, whereas the forecast errors for light and moderate precipitation are smallest in the RNRA experiment. Clearly, the model simulation of this mudslide-inducing rainstorm over Wangmo is improved when using the variational method to correct radar reflectivity, and assimilating radar reflectivity and radial velocity.

To disclose the impact of radar radial velocity and reflectivity data assimilation in LAPS and the variational method to correct the radar reflectivity, we focus on comparing NORA, RA and RNRA. In order to better explain the model's capability in simulating the mudslide-inducing rainstorm over Wangmo in the three experiments, we calculated the average hourly precipitation over the rainstorm region of Wangmo. The results (Fig. 7) indicate that precipitation mainly occurred from nighttime on 5 June to early morning on 6 June. Heavy precipitation lasted from 1500 UTC to 2200 UTC, and the extremely heavy precipitation occurred from 1500
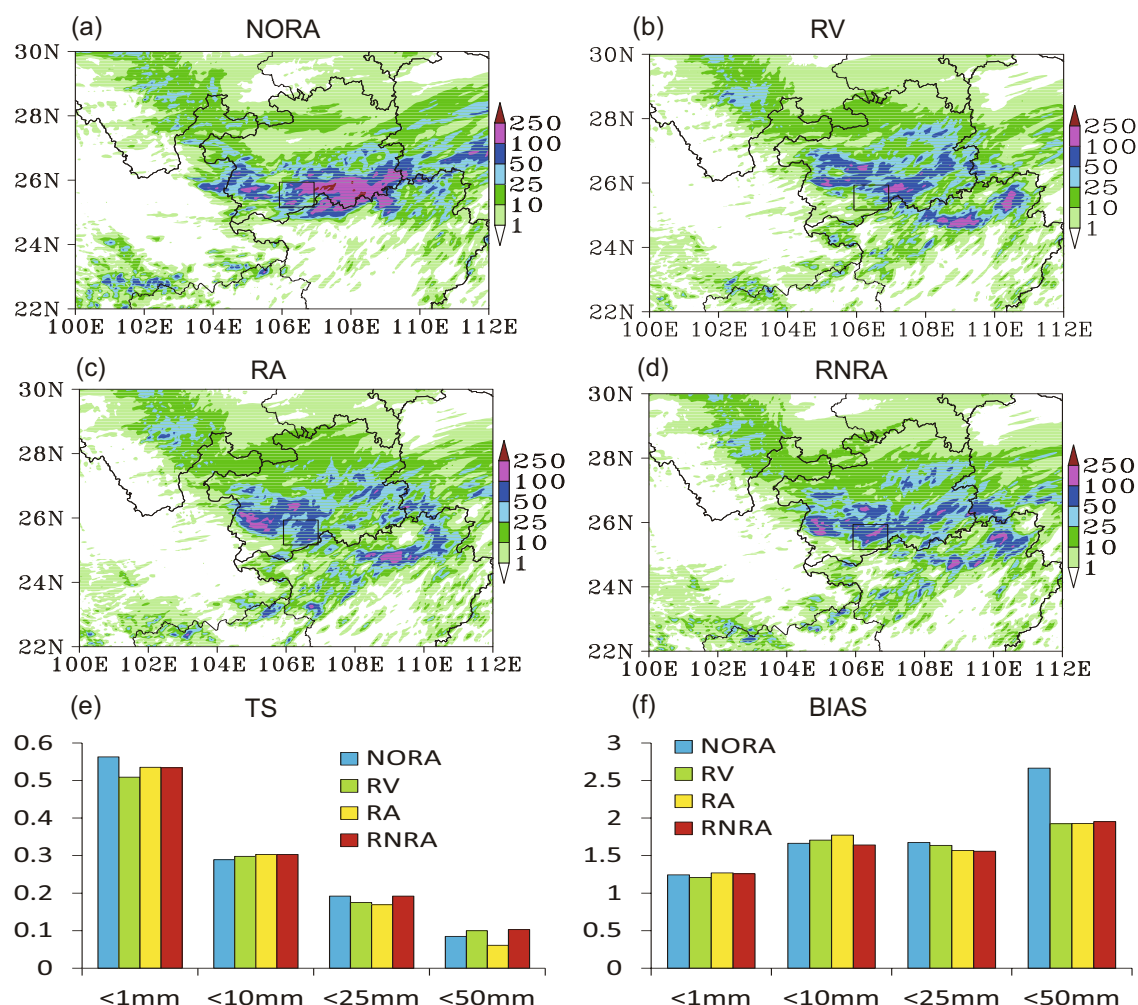
Fig. 6. The 24-h accumulated precipitation for the period 1200 UTC 5 June 2011 to 0000 UTC 6 June 2011 simulated in (a) NORA, (b) RV, (c) RA and (d) RNRA (units: mm). The black solid square represents precipitation over the Wangmo area of the rainstorm. (e, f) The 24-h precipitation forecast threat scores (TS).

UTC to 1800 UTC, with the largest value of 28 mm h^{-1} at 1600 UTC. All three experiments reproduce the observed evolution of precipitation well, which is mainly concentrated over the last 12 hours of the model simulation. Compared with NORA, the temporal evolution of the hourly precipitation simulated in RA is closer to observation. However, note that the maximum precipitation simulated in NORA and RA occurred during the period from 1800 UTC to 2100 UTC, whereas in RNRA it occurred during 1600–1800 UTC. Clearly, the RNRA simulation is more consistent than RONA and RA with observations, which indicates that the variational correction method can improve the model's simulation of the hourly evolution of precipitation.

4.5. *Impact of the WRF–LAPS model simulation physical variables results*

In addition to the verification of precipitation simulation, the simulation of physical variables involved in precipitation processes is also an important issue in the evaluation of model performance. In this section, area-average hourly vorticity,

divergence, and water vapor fluxes are calculated over the Wangmo region. The dynamical processes and the evolution of the water vapor condition over Wangmo simulated by the three experiments are compared to assess the effects of radar reflectivity correction by the variational method. Figure 8 shows time–height cross sections of the area-average evolution of vorticity, divergence, and water vapor flux simulated by the three experiments. It shows that the maximum precipitation occurred during the period 1500–2200 UTC (Fig. 8a). Compared with the results of the other two experiments, the vertical distribution and evolution of the above physical variables simulated in RNRA, which includes information corrected by the variational method, are more consistent with precipitation. During 1500–2200 UTC, positive vorticity simulated in RNRA extends from lower levels to upper levels. At 1600 UTC, the time with heaviest precipitation, the positive vorticity extends up to the top of the model. In contrast, positive vorticity simulated in the other two experiments remains at lower levels during the entire integration period. Divergence simulated in the three experiments is neg-
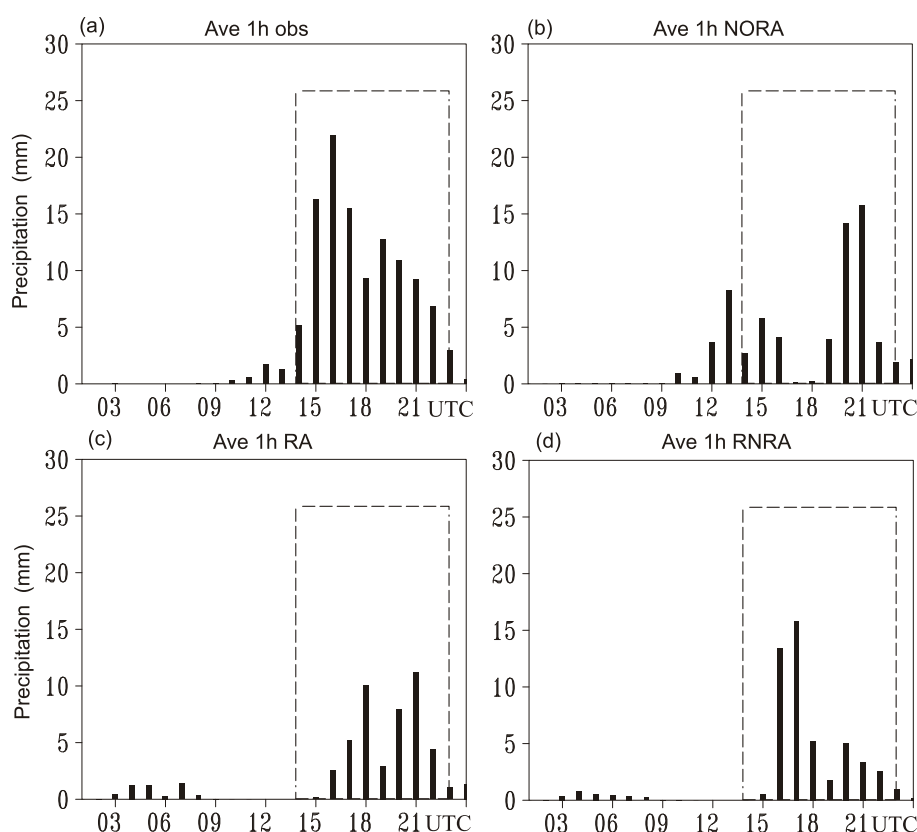
Fig. 7. Area-average hourly precipitation over the rainstorm region of Wangmo from 0000 UTC 5 June to 0000 UTC 6 June 2011: (a) observations; (b) NORA simulation; (c) RA simulation; (d) RNRA simulation (units: mm). The black dotted rectangle represents the time period of the strong precipitation.

ative at lower levels and positive at higher levels. In particular, at 1600 UTC, when the heaviest precipitation occurred, both RA and RNRA produce significant negative divergence below 500 hPa, and the center of the negative divergence is located at 700 hPa. Note that the central negative divergence is much stronger in the RNRA result than that in the RA result, while the central positive divergence at 300 hPa is also stronger in the RNRA simulation than in the RA simulation. This result suggests that at the time of heavy precipitation, distinct low-level convergence and high-level divergence exists in the RNRA simulation. During 1500–2200 UTC, compared with the results from the other experiments, the RNRA experiment produces an area of significant water vapor flux, which is more intense and lasts longer than in the other simulations. The evolution of water vapor flux simulated in RNRA is also more consistent with the evolution of precipitation than in the other two experiments. The above results clearly indicate that the simulation of water vapor transport in the RNRA experiment is better than in the other two experiments. Apparently, with the variational correction of radar reflectivity based on hourly precipitation observations, basic elements and cloud physical variables in the initial conditions of the model can better represent the actual situation, which helps to improve the model's simulation of important physical variables. As a result, the dynamic processes and at-

mospheric moisture transport simulated by the model become more consistent with observation.

4.6. WRF–LAPS model precipitation forecast sensitivity to different initial states of assimilation experiments

From the analysis in section 4.4, in some southeastern portions of the model domain the precipitation is overestimated in the four numerical experiments for this case. Radar reflectivity data at different levels is corrected, separately, and assimilated using LAPS to test whether the overestimated precipitation in these areas can be removed. Three experiments of radar reflectivity data at low (1000–850 hPa), low-mid (700–500 hPa) and high (300–100 hPa) levels, corrected using this variational method, are performed—named EXP1, EXP2 and EXP3, respectively. The parameters of the three experiments are the same as those mentioned in section 3. The purpose of these experiments is to further study the impact and the problem by correcting radar reflectivity data at different levels with this variational method. What we find is that similar results are again produced, based on comparison of the 24-h accumulated precipitation simulated by the three experiments (Fig. 9) and those in rainfall observations (Fig. 1a); as in NORA, RV, RA and RNRA, they cannot remove the overestimated precipitation in Guangxi Province. Variational correction of radar reflectivity at different levels can
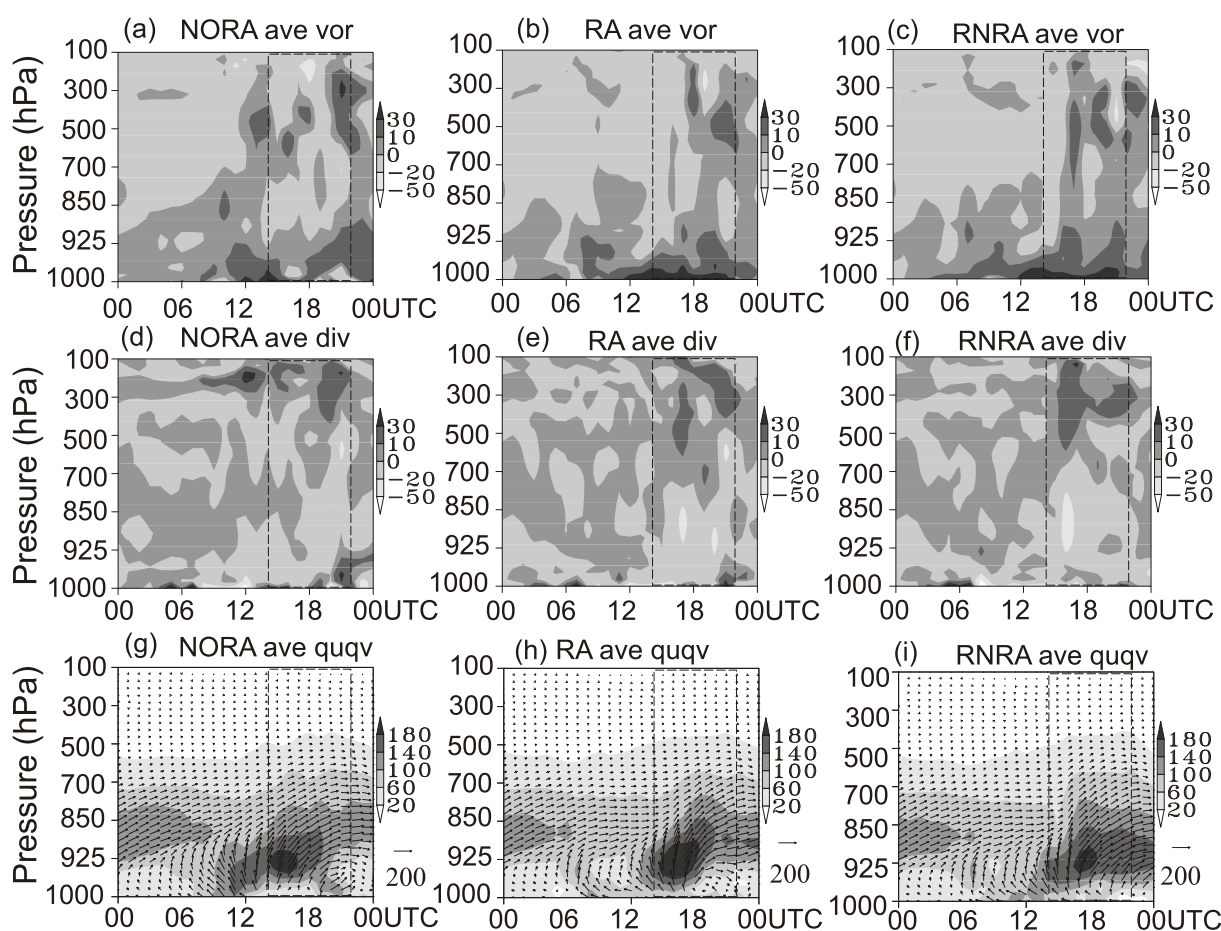
Fig. 8. Area-average (a–c) vorticity (units: 10^5 s^{-1}), (d–f) divergence (units: 10^5 s^{-1}), and (g–i) water vapor flux [units: 10^{-3} g (m s$^{-1})^{-1}$ kg^{-1}]: (a, d, g) NORA simulation; (b, e, h) RA simulation; (c, f, i) RNRA simulation. The black dotted rectangle represents the time period of the strong precipitation.

affect the precipitation forecast over the observed rainstorm area. A more comprehensive analysis of the results will be presented in a follow-up paper.

From all the experiments in which radar data are assimilated by LAPS, the problem of overestimation in the southeastern portion of the model domain for this case cannot be solved effectively. It is possible that the radar data of this area for this case have little effect on the background fields of LAPS. Other rainstorm cases need to be studied to shed further light on the situation.

5. Summary and discussion

This paper describes in detail the development of a variational method to correct radar reflectivity based on hourly ground precipitation observations. There are various types of operational Doppler radar with different detection ranges and horizontal resolutions located in Southwest China, where the terrain is complex, and so the variational method is used to improve the quality of radar reflectivity in this region. Experiments are carried out in which different radar data assimilated by LAPS are applied in a mudslide-inducing rainstorm simulation. The role of radar data assimilation with the vari-

ational method is studied.

The variational method developed in this study can lead to large corrections for radar reflectivity over the rainfall area. The temporal evolution of the variational corrected radar reflectivity is more consistent with the evolution of observed precipitation. When assimilated by LAPS, a better description of the cloud water distribution may be provided, and the cloud water analysis may be improved, over the rainfall area. The LAPS-outputted cloud microphysical variables represent the convection-related cloud water distribution well over the precipitation area, and provide hydrometeors that are consistent with real-time precipitation for the model's initial condition. An initial state that can reasonably describe the atmospheric condition and cloud physics is generated.

Compared with other experiments, after correction by the variational method using hourly ground precipitation observations, the radar reflectivity can improve the simulation performance of the hourly evolution of precipitation and physical parameters and make the simulated dynamic configuration and atmospheric moisture transport processes more consistent with the actual situation over the area of the heavy rainfall center.

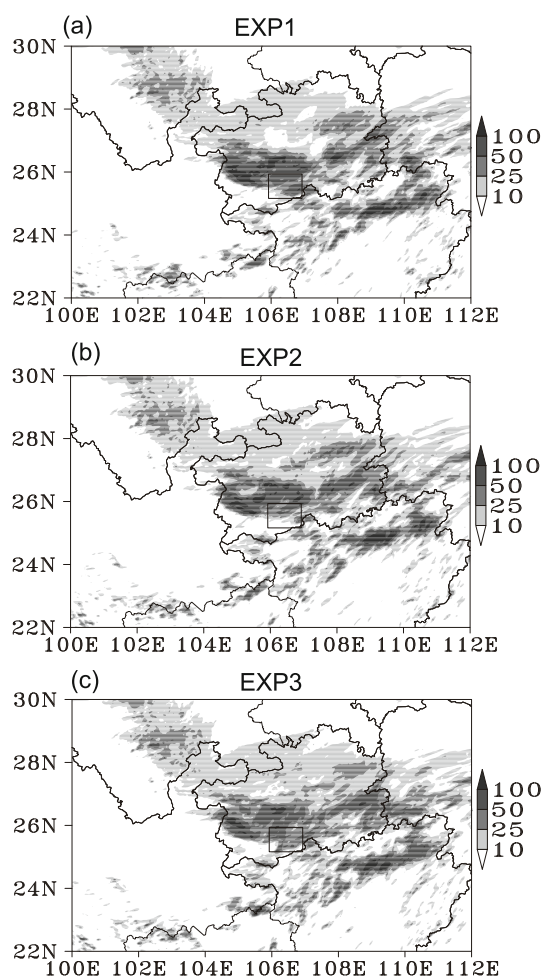Our conclusions here are mainly based on this single case,

Fig. 9. The 24-h accumulated precipitation for the period 1200 UTC 5 June 2011 to 0000 UTC 6 June 2011 simulated in (a) EXP1, (b) EXP2, and (c) EXP3 (units: mm). The black solid bars represent precipitation over the Wangmo area of the rainstorm.

and a number of difficulties with correcting the radar reflectivity factor using this variational method still exist. How to ensure the optimum coefficients of *a* and *b* at each level in the Z–I relationship is key to obtaining better variational correction results. Radar reflectivity is directly assimilated in the LAPS cloud analysis to give cloud fractions that are used in the LAPS moisture analysis. The variables such as humidity, temperature, wind and pressure are adjusted in the LAPS balance analysis to give the model initial fields. The parameters in the LAPS balance analysis may need to be tested. More case studies will be needed to draw more reliable conclusions. Still, we believe our case study represents an important step towards the goal to better assimilate operational Doppler radar data in China.

REFERENCES

Albers, S.C, 1995: The LAPS wind analysis. *Wea. Forecasting*, **10**(2), 342–352.

Albers, S. C., J. A. McGinley, D. L. Birkenheuer, and J. R. Smart, 1996: The Local Analysis and Prediction System (LAPS): Analyses of clouds, precipitation, and temperature. *Wea. Forecasting*, **11**(3), 273–287.

Barker, D. M., W. Huang, Y.-R. Guo, A. J. Bourgeois, and Q. N. Xiao, 2004: A three-dimensional variational data assimilation system for MM5: Implementation and initial results. *Mon. Wea. Rev.*, **132**(4), 897–914.

Birkenheuer, D., 1999: The effect of using digital satellite imagery in the LAPS moisture analysis. *Wea. Forecasting*, **14**(5), 782–788.

Chiang, Y.-M., F.-J. Chang, B. J.-D. Jou, and P.-F. Lin, 2007: Dynamic ANN for precipitation estimation and forecasting from radar observations. *J. Hydrol.*, **334**(1–2), 250–261.

Hu, M., M. Xue, and K. Brewster, 2006a: 3DVAR and cloud analysis with WSR-88D Level-II data for the prediction of the Fort Worth, Texas, tornadic thunderstorms. Part I: Cloud analysis and its impact. *Mon. Wea. Rev.*, **134**(2), 675–698.

Hu, M., M. Xue, J. D. Gao, and K. Brewster, 2006b: 3DVAR and cloud analysis with WSR-88D Level-II data for the prediction of the Fort Worth, Texas, tornadic thunderstorms. Part II: Impact of radial velocity analysis via 3DVAR. *Mon. Wea. Rev.*, **134**(2), 699–721.

IPCC, 2001: *Climate Change 2001: The Scientific Basis. Contribution of Working Group 1 to the Third Assessment Report of the Intergovernmental Panel on Climate Change*, J. T. Houghton et al., Eds., Cambridge University Press, Cambridge, UK, and New York, USA, 881 pp

Li, H.-L., C.-G. Cui, Z.-B. Wang, X.-F. Wang, and Y.-C. Xie, 2009: A study on application of Dopplar radar data in LAPS. *Plateau Meteorology*, **28**(6), 1443–1452. (in Chinese)

Li, Q., X. P. Cui, and J. Cao, 2014: Observational analysis and numerical simulation of a heavy rainfall event in Sichuan province. *Chinese Journal of Atmospheric Sciences*, **38**(6), 1095–1108. (in Chinese)

Liu, R.-X., H.-B. Chen, D.-H. Chen, and G.-Q. Xu, 2014: A case study of impact of FY-2C satellite data in cloud analysis to improve short-range precipitation forecast. *Atmos. Oceanic Sci. Lett.*, **7**(6), 527–533.

Liu, Y. B., and Coauthors, 2008: The operational mesogamma-scale analysis and forecast system of the U.S. army test and evaluation command. Part I: Overview of the modeling system, the forecast products, and how the products are used. *J. Appl. Meteor. Climatol.*, **47**(4), 1077–1092.

McGinley, J. A., S. C. Albers, and P. A. Stamus, 1991: Validation of a composite convective index as defined by a real-time local analysis system. *Wea. Forecasting*, **6**(3), 337–356.

Qu, Y. M., R. H. Cai, L. J. Zhu, G. J. Wang, and H. Y. Wang, 2012: Application of cloud analysis system to Typhoon Molave Simulation. *Journal of Applied Meteorological Science*, **23**(5), 551–561. (in Chinese)

Reisner, J., R. M. Rasmussen, and R. T. Bruintjes, 1998: Explicit forecasting of supercooled liquid water in winter storms us-

ing the MM5 mesoscale model. *Quart. J. Roy. Meteor. Soc.*, **124**(548), 1071–1107.

Shen, Y., and A. Y. Xiong, 2015: Validation and comparison of a new gauge-based precipitation analysis over mainland China. Int. *J. Climatol.*, **36**, 252–265, doi: 10.1002/joc.4341.

Shaw, B. L., J. A. McGinley, and P. Schultz, 2001: Explicit initialization of clouds and precipitation in mesoscale forecast models. *14th Conf. on Numerical Weather Prediction*, Ft. Lauderdale, FL, Amer. Meteor. Soc.

Xie, Y. F., S. Albers, H. L. Jiang, D. Birkenheuer, and Z. Toth, 2013: Variational cloud analysis using CRTM in a multiscale analysis. *Proc. 93rd Annual Meeting*, Austin, TX, Amer. Meteor. Soc.

Xu, S. Z., Q. Jin, Y. J. Xiao, and J. Li, 2005: Mesoscale analysis of a heavy rainfall causing mud-rock flow. *Meteorological Science and Technology*, **33**(3), 240–244. (in Chinese)

Xue, M., D. H. Wang, J. D. Gao, K. Brewster, and K. K. Droegemeier, 2003: The Advanced Regional Prediction System (ARPS), storm-scale numerical weather prediction and data assimilation. *Meteor. Atmos. Phys.*, **82**(1–4), 139–170.

Zhang, L. P., L. Li, A. Z. Ye, and J. Xia, 2007: Contrast research on precision of estimating regional precipitation with weather radar and rain gauge. *Engineering Journal of Wuhan University*, **40**(1), 1–5. (in Chinese)

Zhang, Y., H. C. Lei, X. B. Pan, C. M. Wang, and Y. Q. Xie, 2009: Study on cloud micro-physical processes and precipitation formative mechanisms of a mesoscale convective system in Meiyu front in June 2004. *Scientia Meteorologica Sinica*, **29**(4), 434–446. (in Chinese)

Zhao, Y. C., and C. G. Cui, 2010: A study of rainstorm process triggering Zhouqu extremely mudslide on 8 August 2010. *Torrential Rain and Disasters*, **29**(3), 289–295. (in Chinese)

Zheng, L. L., J. H. Sun, X. L. Zhang and C. H. Liu, 2013: Organizational modes of mesoscale convective systems over Central East China. *Wea. Forecasting*, **28**(5), 1081–1098.